Conditional statistics in a planar liquid jet with a second-order chemical reaction

Tomoaki Watanabe[a,b,1,*], Yasuhiko Sakai[a], Kouji Nagata[a], Osamu Terashima[a], Takashi Kubo[c]

[a] *Department of Mechanical Science and Engineering, Nagoya University, Nagoya 464-8603, Japan*
[b] *Research Fellow of the Japan Society for the Promotion of Science*
[c] *Faculty of Science and Technology, Meijo University, Nagoya 468-8502, Japan*

Abstract

Conditional statistics, conditioned on mixture fraction, are experimentally investigated in a planar liquid jet with a second-order isothermal chemical reaction A + B → R. Reactants A and B are contained in the jet and ambient flows, respectively, and are supplied into the test section under the non-premixed condition. Streamwise velocity, mixture fraction and concentration of all reactive species are simultaneously measured by using an I-type hot-film probe and an optical fibre probe based on light absorption spectrometry. The cross-streamwise profiles of conditional mean concentrations and conditional mean reaction rate show that the conditional mean concentrations and the conditional mean reaction rate near the jet exit change with the cross-streamwise position, whereas they are independent of the cross-streamwise position in the downstream regions. On the jet centreline, the conditional mean reaction rate has a peak value on the condition that the

*Corresponding author (+81-052-789-4487)
Email address: watanabe.tomoaki@c.nagoya-u.jp (Tomoaki Watanabe)

conditional mean concentration of product R has a peak value. A comparison between the conditional mean reaction rate and the covariance of conditional concentration fluctuations shows that the covariance of conditional concentration fluctuations is so small that a first moment closure model for the conditional mean reaction rate is valid. The conditional mean streamwise velocity is almost linear to the mixture fraction for small mixture fraction fluctuations. The conditional scalar dissipation rate is calculated from the budget of the conditional moment closure equation. The results show that the conditional scalar dissipation rate has a single peak value in the upstream region, whereas in the downstream region, it has two peaks for the large and small mixture fraction values. The conventional mean scalar dissipation rate is calculated from the probability density function of the mixture fraction and the conditional scalar dissipation rate. The conventional mean scalar dissipation rate on the jet centreline decreases in the downstream direction as $(x^*)^{-2.9}$ (where x^* is the distance from the virtual origin), which is almost the same as that expected from scaling arguments.
Keywords: Turbulent Transfer, Chemical Reaction, Jet, Conditional Moment Closure, Mixing

1. Introduction

Chemical reactions in the environment or in industrial equipment often occur in turbulent flows. In non-premixed systems, chemical reactions occur with turbulent mixing of reactants. Turbulent flows have a great influence on chemical reactions and mixing of chemical substances [1], and understanding turbulent flows with chemical reactions will help us develop numerical

methods to predict them. Therefore, elucidating the mechanism of chemical reactions in turbulent flows is desired. Numerical methods for turbulent reactive flows [2] are important for predicting the efficiency of combustors or chemical reactors and for understanding pollutant formation in the atmosphere.

Direct numerical simulation (DNS), in which the governing equations (e.g., the continuity equation, the Navier–Stokes equations or the equations for energy and mass transfer) are numerically solved without any models, provides the most accurate and reliable solutions. However, because of the high computational cost of DNS, its application is limited to flows at low Reynolds numbers and in simple geometries. DNS has been employed for investigating chemical reactions in turbulent flows and developing models for turbulent reactive flows (e.g., [3, 4, 5, 6, 7, 8]).

From a practical point of view, the Reynolds-averaged approach, in which the Reynolds-averaged governing equations are solved by using turbulent models, is useful for predicting turbulent flows because of its low computational cost. To apply the Reynolds-averaged approach to turbulent reactive flows, models for the turbulent mass flux and the mean chemical reaction rate are required to solve averaged equations for reactive scalar transfer. The gradient diffusion model [9] is often used to model the turbulent mass flux of reactive species [2, 10], and various models have been proposed for the mean chemical reaction rate [10, 11, 12, 13]. However, it has been pointed out that the gradient diffusion hypothesis is largely influenced by chemical reactions [14, 15, 16, 17]. Additionally, models for the mean chemical reaction rate are valid only for particular flows. Therefore, the Reynolds-averaged approach is

unsuited for reactive flows unless it is used with another numerical method to treat the effect of chemical reactions.

The conditional moment closure (CMC) method [18, 19] was developed to simulate turbulent reactive flows. Because the CMC method is like the Reynolds-averaged approach, its computational cost is not high, and it can be applied to various flows and chemical reactions. Masri et al. [20] measured the temperature and concentrations of reactive species in a non-premixed jet flame of methanol, and showed that temperature and concentrations of reactive species strongly depend on the mixture fraction, which can be defined by the normalized concentration of nonreactive species. Thus, for the case in which reactants are mixed and react in a non-premixed system, the variables related to the chemical reactions depend on the mixture fraction. In the CMC method, turbulent reactive flows are simulated by solving the transport equations for conditional mean concentrations, conditioned on the mixture fraction. The conditional mean concentration of species α (Q_α), conditioned on the mixture fraction ξ, is defined as

$$Q_\alpha \equiv \langle \Gamma_\alpha \mid \xi = \eta \rangle \equiv \langle \Gamma_\alpha \mid \eta \rangle, \tag{1}$$

where Γ_α is the instantaneous concentration of species α, $\langle\ \rangle$ denotes an ensemble average, $\langle \mid * \rangle$ denotes an ensemble average conditioned on $*$ and η is the sample space variable for ξ. The transport equation for Q_α was derived by Klimenko [21] and Bilger [18] and can be written as

$$\frac{\partial Q_\alpha}{\partial t} + \langle U_i \mid \eta \rangle \frac{\partial Q_\alpha}{\partial x_i} - \langle N \mid \eta \rangle \frac{\partial^2 Q_\alpha}{\partial \eta^2} = \langle W_\alpha \mid \eta \rangle, \tag{2}$$

where U_i is the instantaneous i direction velocity, W_α is the production rate of species α by chemical reactions and N is the scalar dissipation rate, which

is defined by

$$N \equiv D \frac{\partial \xi}{\partial x_i} \frac{\partial \xi}{\partial x_i}. \tag{3}$$

Here, D is the molecular diffusivity, which is often assumed to be independent of species. Solving Eq. (2) requires models for the conditional mean velocity $\langle U_i \mid \eta \rangle$, the conditional scalar dissipation rate $\langle N \mid \eta \rangle$ and the conditional mean reaction rate $\langle W_\alpha \mid \eta \rangle$. In the Reynolds-averaged approach, it is required to model the conventional mean reaction rate (where "conventional mean" denotes a time average or an ensemble average). Even for a simple second-order isothermal reaction, modelling the conventional mean reaction rate is not easy because concentration fluctuations arising from turbulence greatly contribute to the mean reaction rate and their contributions are not easy to predict [22, 23]. Because concentration fluctuations from the conditional mean concentrations often have only a negligible contribution to the conditional mean reaction rate [18], the models for the conditional mean reaction rate $\langle W_\alpha \mid \eta \rangle$ are simpler than those for the conventional mean reaction rate. This is one of the advantages of using the CMC method.

To verify the numerical accuracy of the CMC method and the models for the unclosed terms used in the CMC method, it is important to investigate conditional statistics in turbulent reactive flows. Experimentally measuring conditional statistics in reactive flows requires simultaneous measurement of the mixture fraction and other quantities. Conditional moments of the temperature and the mass fraction of reactive species have been measured in jet flames by Masri et al. [20], Barlow et al. [24, 25] and others. In gas flows, many measurements of conditional statistics have been conducted. Bilger et al. [14] measured reactive concentrations in a scalar mixing layer

with a second-order chemical reaction and investigated the conditional mean concentrations of reactive species [18]. Li and Bilger [26] measured the covariance of conditional concentration fluctuations in a reactive scalar mixing layer. Brown and Bilger [27] measured the conditional statistics in a reactive plume in grid turbulence. Most of conditional statistics measurements have been conducted in the gas phase, in which diffusion and mixing of reactive species are characterised by a lower Schmidt number (or Prandtl number) than those in the liquid phase. DNS has been used to investigate the conditional statistics and the models used for the CMC method (e.g., [6, 28, 29]). However, DNS can be applied only to flows at low Schmidt number ($Sc = \nu/D$, where ν is the kinematic viscosity and D is the molecular diffusivity) because the smallest scale of scalar fluctuations, which is called the Batchelor scale, becomes small, being proportional to $Sc^{-1/2}$ [30]. Thus, there have been few investigations of conditional statistics in liquid flows. Most measurements of conditional statistics of reactive concentration have been conducted in flames, in which the Damköhler number, which is the ratio of flow to reaction time scales, is very large.

The scalar dissipation rate [31] is a key variable in turbulent reactive flows, especially for fast chemical reactions. When fast chemical reactions occur in a non-premixed system, the chemical reaction rate strongly depends on the scalar dissipation rate [32]. Models for the statistics of the scalar dissipation rate [33, 34, 35] are important for numerical simulations of reactive flows. However, measurement of the conditional scalar dissipation rate is a challenging problem, especially in liquid flows because a spatial resolution comparable to the Batchelor scale is required to accurately perform the mea-

surement [36]. In jet flows in the gas phase, the scalar dissipation rate has been measured by Su and Clemens [37], Karpetis and Barlow [38] and Su et al [39]. In a liquid jet, Kailasnath et al. [40] measured the scalar dissipation rate. However, the smallest scale of scalar fluctuations was not resolved in many of the previous scalar dissipation rate measurements.

The purpose of this study is to investigate the conditional statistics in a reactive jet at high Sc. Concentrations of reactive species and velocity are simultaneously measured in a planar liquid jet with a second-order isothermal reaction to investigate the conditional statistics. By using the measurement results of conditional statistics, the conditional scalar dissipation rate can be estimated from the budget of Eq. (2). This method to estimate the conditional scalar dissipation rate requires measurements of the conditional average of concentration, velocity and reaction rate. Because these conditional statistics are less sensitive to the spatial resolution of measurement than is the scalar dissipation rate [36], it is possible to estimate the conditional scalar dissipation rate from Eq. (2) even at high Sc. The conditional statistics have been investigated in turbulent reactive flows at low Sc, such as turbulent jet flames, and the models used in the CMC methods were verified based on those experimental and numerical results. Our experiments are conducted at high Sc and small Damköhler number compared with previous experiments on turbulent flames. Because of a difficulty of measuring concentrations of reactive species, data on the conditional statistics in reactive flows at high Sc are lacking. Therefore, it remains still unclear whether the models used in the CMC methods are applicable to turbulent reactive flows at high Sc. The present study will reveal the characteristics of the condi-

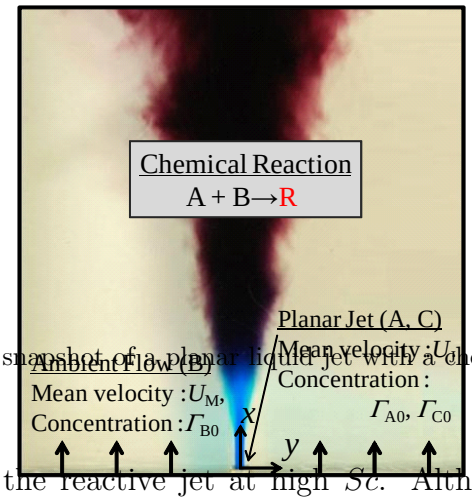

Figure 1: A snapshot of a planar liquid jet with a chemical reaction.

tional statistics in the reactive jet at high Sc. Although previous studies showed that the conditional statistics are almost independent of positions across flows in a mixing layer [18] and a plume [27], we will show that the conditional statistics change in the cross-streamwise direction of the planar jet in the upstream region. The results will be also used for verifying the models used in the CMC methods, and eventually, we will show that some of the models used in reactive flows at low Sc are still useful even for high Sc cases.

In sections 2 and 3, the experiments and the measurement methods are described in detail. The measurement results of the conditional statistics are given in section 4. Finally, the conclusions are summarized in section 5.

2. Experiments

Fig. 1 shows a snapshot of the planar liquid jet with a chemical reaction A + B $\rightarrow$ R investigated in this study. Here, reactant A is 1-naphthol and reactant B is diazotized sulfanilic acid. Product R is 4-(4′-sulphophenylazo)-1-naphthol, briefly referred to as monoazo dyestuff. The chemical reaction rate constant of this reaction is $k = 12\,000$ m^3/(mol·s) [41]. Reactants A and B are contained in the jet and ambient flows, respectively, and are supplied into the test section under the non-premixed condition. The jet flow is injected into the ambient flow through a rectangular slit with a width of $d = 2$ mm and a spanwise length of 40 mm. Acid Blue 9 (blue dyestuff), which is called species C hereafter, is also contained into the jet flow. Species C does not affect the above chemical reaction, and the concentration of nonreactive species C can be considered as a conserved scalar. To keep pH constant in the jet (pH = 10), buffer salt (Na_2CO_3 and $NaHCO_3$) is added into the jet flow. As shown in Fig. 1, the origin of the coordinate system is located at the centre of jet exit. x, y and z denote streamwise, cross-streamwise and spanwise directions, respectively.

The mean velocity at the jet exit is $U_\mathrm{J} = 1.29$ m/s, and the mean velocity of the ambient flow is $U_\mathrm{M} = 0.073$ m/s. The Reynolds number defined by $Re = (U_\mathrm{J} - U_\mathrm{M})d/\nu$ is 2 200. The initial concentrations of species A, B and C are $\Gamma_\mathrm{A0} = 0.4$ mol/m^3, $\Gamma_\mathrm{B0} = 0.2$ mol/m^3 and $\Gamma_\mathrm{C0} = 0.1$ kg/m^3, respectively. The Damköhler number defined by $Da = k(\Gamma_\mathrm{A0} + \Gamma_\mathrm{B0})d/(U_\mathrm{J} - U_\mathrm{M})$ is 11.8. The Schmidt number based on the molecular diffusivity of species C is $Sc \approx 600$. Mehta and Tarbell also conducted the experiments on the reaction of 1-naphthol (A) and diazotized sulfanilic acid (B) [42]. The

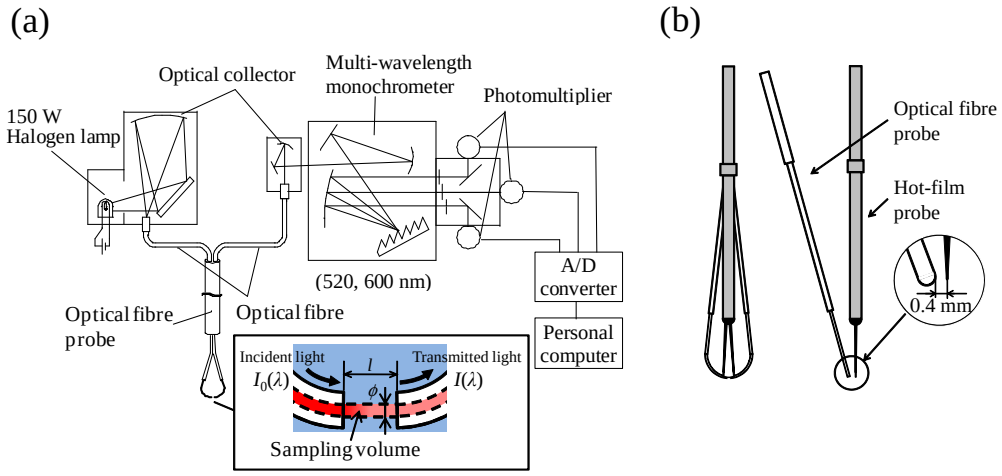

Figure 2: The measurement system. (a) Concentration measurement system. (b) Combined probe for the simultaneous measurements of velocity and concentrations.

initial concentrations of A and B in the present experiments are comparable with those in their experiments. Similar to their experiments, the aqueous solutions of A, B, R, and C are dilute in the present experiments. Because the dilute solutions are used in the experiments, the reactive species A, B, and R and nonreactive dyestuff C are considered to act as passive scalars.

3. Measurement Methods

Concentrations of product R and nonreactive species C and streamwise velocity are simultaneously measured with an optical fibre probe [43] based on light absorption spectrometry and an I-type hot-film probe. The same measurement method is used by the authors [44, 45]. The measurement method is briefly explained below; for further details see [44].

Fig. 2(a) shows the concentration measurement system based on light

absorption spectrometry [46]. Light emitted by a halogen lamp is fed into an optical fibre probe and passes through the sampling volume. Assuming that there is a solution of dyestuff species α at the sampling volume, light of wavelength λ passing the sampling volume decays because of light absorption by species α. From Beer's absorption law, the light intensity of the incident light, $I_0(\lambda)$, and the light intensity of the transmitted light, $I(\lambda)$, are related to the instantaneous concentration of species α ($\mathit{\Gamma}_\alpha$) at the sampling volume as

$$-\ln \frac{I(\lambda)}{I_0(\lambda)} = k_\alpha(\lambda)\mathit{\Gamma}_\alpha. \tag{4}$$

Here, $k_\alpha(\lambda) = l\beta_\alpha(\lambda)$, where l is the length of the light path, and β_α is dependent on λ and the light absorption characteristics of species α. When the solution at the sampling volume contains multiple dyestuffs, $P(\lambda) \equiv -\ln(I(\lambda)/I_0(\lambda))$ is equal to the sum of each $P(\lambda)$ for a solution of single dyestuff. Hence, $P(\lambda_n)$ for a solution containing the product R and species C can be written as

$$P(\lambda_n) \equiv -\ln \frac{I(\lambda_n)}{I_0(\lambda_n)} = k_\mathrm{R}(\lambda_n)\mathit{\Gamma}_\mathrm{R} + k_\mathrm{C}(\lambda_n)\mathit{\Gamma}_\mathrm{C}. \tag{5}$$

After the light passes through the sampling volume, it is split into two wavelengths ($\lambda_1 = 520$ nm and $\lambda_2 = 600$ nm) by a grating spectroscope, and the intensities of the split light are measured by a photomultiplier. $P(\lambda_1)$ and $P(\lambda_2)$ are calculated from the measured light intensities, and $k_\mathrm{R}(\lambda_1)$, $k_\mathrm{R}(\lambda_2)$, $k_\mathrm{C}(\lambda_1)$ and $k_\mathrm{C}(\lambda_2)$ are determined by prior calibration experiments. Then, $\mathit{\Gamma}_\mathrm{R}$ and $\mathit{\Gamma}_\mathrm{C}$ can be obtained by solving Eq. (5).

The mixture fraction ξ is defined by the normalized concentration of

nonreactive species C:

$$\xi \equiv \frac{\Gamma_{\rm C}}{\Gamma_{\rm C0}}. \tag{6}$$

The instantaneous concentrations of reactants A and B are determined from ξ and $\Gamma_{\rm R}$ by using the mass conservation law [14, 47]:

$$\Gamma_{\rm A} = \xi\Gamma_{\rm A0} - \Gamma_{\rm R}, \tag{7}$$

$$\Gamma_{\rm B} = (1-\xi)\Gamma_{\rm B0} - \Gamma_{\rm R}. \tag{8}$$

Instantaneous concentrations for the frozen limit, which corresponds to the limiting case of $k \to 0$, can be derived as follows [14]:

$$\Gamma_{\rm A}^0 \equiv \lim_{k\to 0}\Gamma_{\rm A} = \xi\Gamma_{\rm A0}, \tag{9}$$

$$\Gamma_{\rm B}^0 \equiv \lim_{k\to 0}\Gamma_{\rm B} = (1-\xi)\Gamma_{\rm B0}, \tag{10}$$

$$\Gamma_{\rm R}^0 \equiv \lim_{k\to 0}\Gamma_{\rm R} = 0. \tag{11}$$

Instantaneous concentrations for the equilibrium limit, which corresponds to the limiting case of $k \to \infty$, are derived as follows [14]:

$$\Gamma_{\rm A}^\infty \equiv \lim_{k\to\infty}\Gamma_{\rm A} = (\Gamma_{\rm A0}+\Gamma_{\rm B0})(\xi-\xi_S)H(\xi-\xi_S), \tag{12}$$

$$\Gamma_{\rm B}^\infty \equiv \lim_{k\to\infty}\Gamma_{\rm B} = (\Gamma_{\rm A0}+\Gamma_{\rm B0})(\xi_S-\xi)H(\xi_S-\xi), \tag{13}$$

$$\Gamma_{\rm R}^\infty \equiv \lim_{k\to\infty}\Gamma_{\rm R} = \begin{cases} \Gamma_{\rm A0}\xi & (\xi < \xi_S) \\ \Gamma_{\rm B0}(1-\xi) & (\xi \geq \xi_S) \end{cases}. \tag{14}$$

Here, $\xi_{\rm S}$ is the stoichiometric ratio of reactants in the mixture and is given by

$$\xi_{\rm S} = \frac{\Gamma_{\rm B0}}{\Gamma_{\rm A0}+\Gamma_{\rm B0}}. \tag{15}$$

In the present conditions, $\xi_{\rm S} = 0.333$. The concentrations for the frozen and equilibrium limits are minimum and maximum values of concentrations of

reactive species:

$$\Gamma_{\mathrm{A}}^{\infty} \leq \Gamma_{\mathrm{A}} \leq \Gamma_{\mathrm{A}}^{0}, \tag{16}$$

$$\Gamma_{\mathrm{B}}^{\infty} \leq \Gamma_{\mathrm{B}} \leq \Gamma_{\mathrm{B}}^{0}, \tag{17}$$

$$\Gamma_{\mathrm{R}}^{0} \leq \Gamma_{\mathrm{R}} \leq \Gamma_{\mathrm{R}}^{\infty}. \tag{18}$$

By substituting $\xi = \xi_{\mathrm{S}}$ and $\Gamma_{\mathrm{A}} = \Gamma_{\mathrm{B}} = 0$ in Eq. (7) or (8), the maximum concentration of product R can be obtained; it is given by $\Gamma_{\mathrm{R0}} = \Gamma_{\mathrm{A0}}\Gamma_{\mathrm{B0}}/(\Gamma_{\mathrm{A0}} + \Gamma_{\mathrm{B0}}) = 0.133$ mol/m^3.

For simultaneous measurements of streamwise velocity and concentrations, an optical fibre probe is combined with an I-type hot-film probe (TSI 1210-20W), as shown in Fig. 2(b). The sampling volume of the optical fibre probe is located 0.4 mm away from that of the I-type hot-film probe in the cross-streamwise direction. The diameter of the optical fibre bundle used in the optical fibre probe is $\phi = 0.5$ mm, and the length of the sampling volume is $l = 0.7$ mm (Fig. 2(a)). The length of the sensing element of the hot-film probe is 1.02 mm, and its diameter is 50.8 μm. The spatial resolution of the combined probe is smaller than the Taylor microscale [44]. The effects of the distance between the two probes on measurements have been carefully examined [44]. By using the combined probe, the streamwise velocity and the concentrations of product R and species C can be simultaneously measured in the planar liquid jet. The concentrations of reactants A and B can then be determined from Eqs. (7) and (8). The measurement results of conventional statistics (e.g., mean concentrations, rms values of concentration fluctuations and turbulent mass fluxes of reactive species) were discussed by the authors [44, 45, 48].

The measurement results of the velocity and concentration of C were compared with the DNS of planar jets [49], and it was confirmed that the development of mean flow and nonreactive scalar fields and the self-similar profiles of the velocity and concentration statistics show good agreement between the experiment and the DNS [50, 51, 52].

4. Results and Discussion

4.1. Scatter plots of concentration of reactive species

Fig. 3 shows the scatter plots of $\Gamma_\alpha/\Gamma_{\alpha 0}$ versus the mixture fraction at $x/d = 10$ and 40 on the jet centreline and $y/b_\xi = 1$ at $x/d = 10$, where b_ξ is the jet half-width based on the mean mixture fraction. The conditional mean concentrations for the frozen and equilibrium limits can be derived by substituting $\xi = \eta$ in Eqs. (9)–(14). Fig. 3 also shows the conditional mean concentration $Q_\alpha/\Gamma_{\alpha 0}$ and the conditional mean concentration for the frozen and equilibrium limits. The scatter plots of $\Gamma_\alpha/\Gamma_{\alpha 0}$ are distributed around the conditional mean concentration and between the conditional mean concentrations for the frozen and equilibrium limits, as expected from Eqs. (16), (17) and (18). As shown in Figs. 3(a) and (b), the instantaneous concentrations of reactive species are close to those for the frozen limit at $x/d = 10$ on the jet centreline, and they are close to the concentrations for the equilibrium limit at $x/d = 40$ on the jet centreline because of the progress of the chemical reaction. Comparison of Figs. 3(a) and (c) shows that the concentration fluctuation from the conditional mean value becomes large away from the jet centreline.

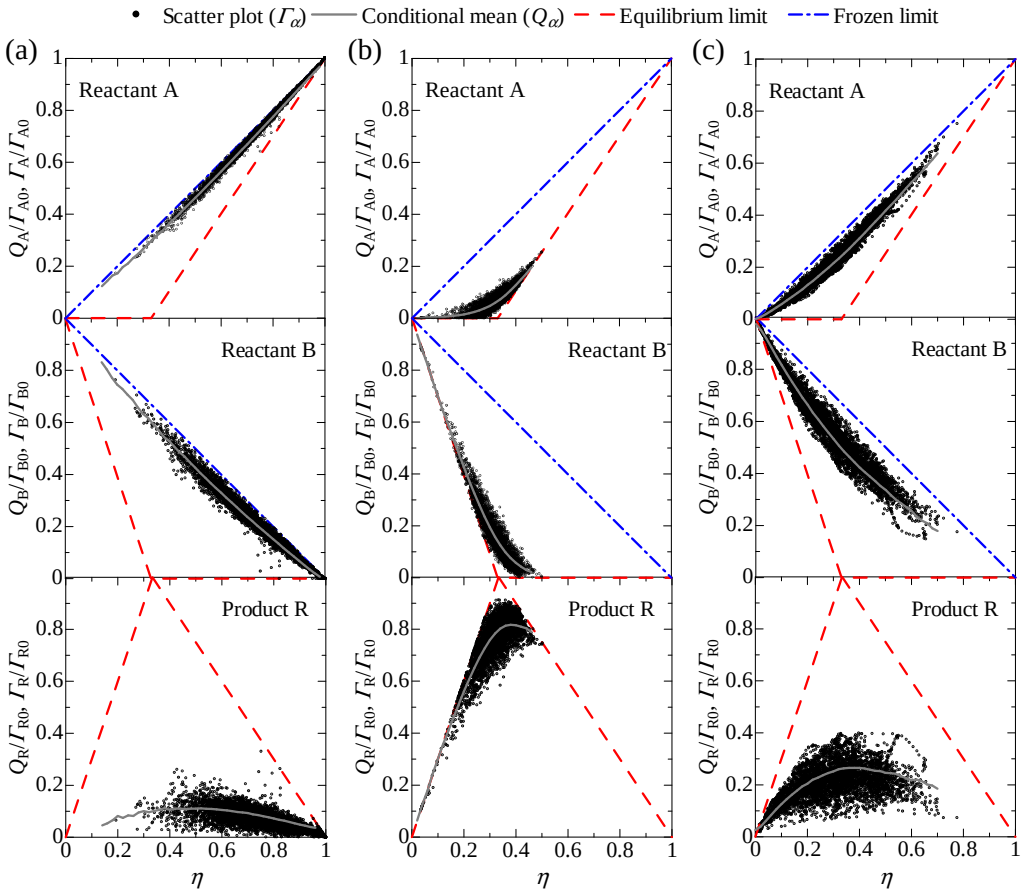

Figure 3: Scatter plots of reactive concentration Γ_α, the conditional mean concentration of reactive species Q_α, Q_α for the frozen limit and Q_α for the equilibrium limit. (a) $x/d = 10$ on the jet centreline. (b) $x/d = 40$ on the jet centreline. (c) $y/b_\xi = 1$ at $x/d = 10$.

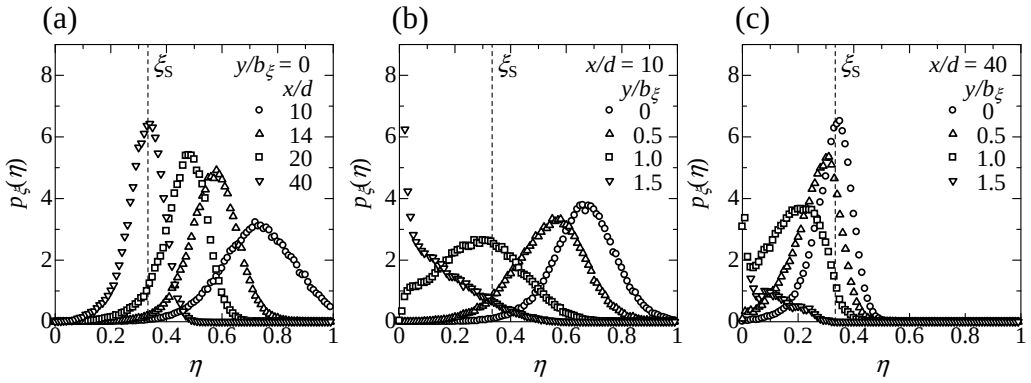

Figure 4: Probability density functions of the mixture fraction. (a) Streamwise variation on the jet centreline. (b) Cross-streamwise variation at $x/d = 10$. (c) Cross-streamwise variation at $x/d = 40$.

4.2. Probability density function of the mixture fraction

In the CMC method, the conventional mean concentration $\langle \Gamma_\alpha \rangle$ is calculated from Q_α and the probability density function of ξ as follows:

$$\langle \Gamma_\alpha \rangle = \int_0^1 \langle \Gamma_\alpha \mid \eta \rangle p_\xi(\eta) d\eta, \tag{19}$$

where $p_\xi(\eta)$ is the probability density function of the mixture fraction. Figs. 4(a), (b) and (c) show the streamwise variation of $p_\xi(\eta)$ on the jet centreline and the cross-streamwise variations of $p_\xi(\eta)$ at $x/d = 10$ and 40. In Fig. 4, $\xi_S = 0.333$ is shown by the broken line. Near the jet centreline in the upstream region ($x/d = 10$, 14 and 20 in Fig. 4(a) and $y/b_\xi = 0$ and 0.5 in Fig. 4(b)), $p_\xi(\eta)$ has a peak at a mixture fraction greater than ξ_S. In the other region, the mixture fraction is small, and $p_\xi(\eta)$ has a peak at a mixture fraction of less than or equal to ξ_S.

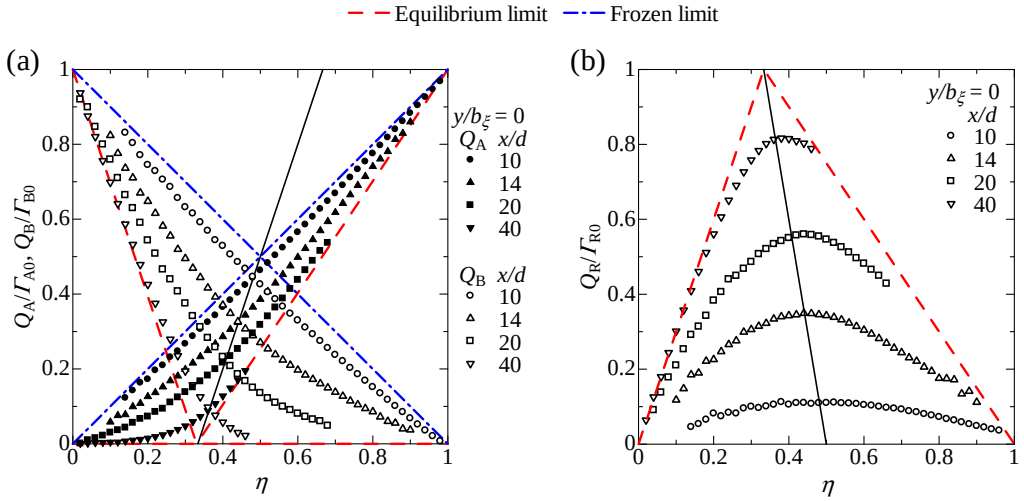

Figure 5: Streamwise variation of conditional mean concentrations of reactive species on the jet centreline. Black solid line: Eqs. (30) and (31). (a) Reactants A and B. (b) Product R.

4.3. Conditional statistics of reactive concentration

Fig. 5 shows $Q_\alpha/\Gamma_{\alpha 0}$ and the conditional mean concentrations for the frozen and equilibrium limits on the jet centreline. At $x/d = 10$, $Q_\alpha/\Gamma_{\alpha 0}$ is close to the concentrations for the frozen limit because the chemical reaction does not proceed enough to significantly change the concentrations of reactive species. In the downstream direction, Q_A and Q_B decrease, and Q_R increases as the chemical reaction progresses, and they approach the conditional mean concentrations for the equilibrium limit. For η much smaller than $\xi_\mathrm{S} = 0.333$ at $x/d = 40$ on the jet centreline, Q_α is almost the same as the conditional mean concentrations for the equilibrium limit, because the chemical reaction easily reaches an equilibrium state after most of reactant B, whose concentration is small for small η, is consumed.

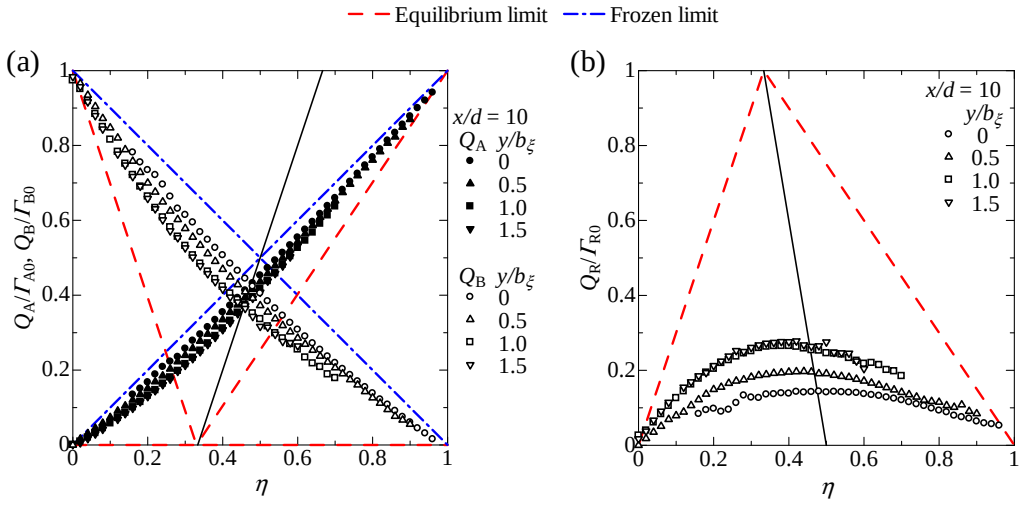

Figure 6: Cross-streamwise variation of conditional mean concentrations of reactive species at $x/d = 10$. Black solid line: Eqs. (30) and (31). (a) Reactants A and B. (b) Product R.

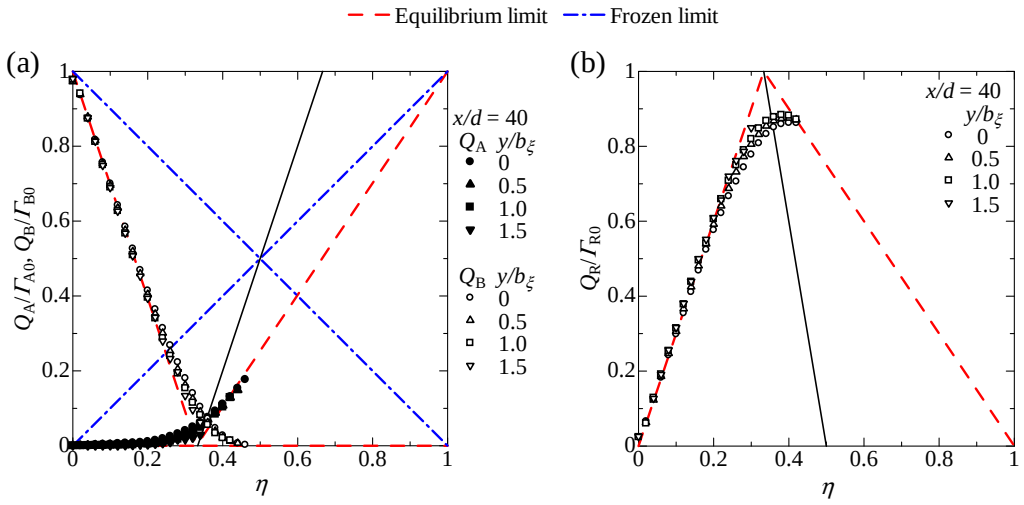

Figure 7: Cross-streamwise variation of conditional mean concentrations of reactive species at $x/d = 40$. Black solid line: Eqs. (30) and (31). (a) Reactants A and B. (b) Product R.

For the second-order chemical reaction $\mathrm{A} + \mathrm{B} \rightarrow \mathrm{R}$, the production rate of product R by the chemical reaction, W_{R}, is given by

$$W_{\mathrm{R}}(\Gamma_{\mathrm{A}}, \Gamma_{\mathrm{B}}) = k\Gamma_{\mathrm{A}}\Gamma_{\mathrm{B}}. \tag{20}$$

The concentration fluctuation γ''_α from the conditional mean concentration is defined by

$$\Gamma_\alpha \equiv Q_\alpha + \gamma''_\alpha. \tag{21}$$

Taking the conditional average of the Taylor expansion for W_{R} around $(\Gamma_{\mathrm{A}}, \Gamma_{\mathrm{B}}) = (Q_{\mathrm{A}}, Q_{\mathrm{B}})$ and neglecting the high-order terms yield the following equation [19]:

$$\langle W_{\mathrm{R}} \mid \eta \rangle = kQ_{\mathrm{A}}Q_{\mathrm{B}} + k\langle \gamma''_{\mathrm{A}}\gamma''_{\mathrm{B}} \mid \eta \rangle. \tag{22}$$

The first moment closure for the conditional mean reaction rate can be obtained by assuming that the conditional correlation term $\langle \gamma''_{\mathrm{A}}\gamma''_{\mathrm{B}} \mid \eta \rangle$ is small compared with $Q_{\mathrm{A}}Q_{\mathrm{B}}$. In the first moment closure, the conditional mean reaction rate is given by

$$\langle W_{\mathrm{R}} \mid \eta \rangle = kQ_{\mathrm{A}}Q_{\mathrm{B}}. \tag{23}$$

By using Eqs. (7) and (8), the conditional mean concentrations of reactants A and B can be related to the conditional mean concentration of product R as

$$\hat{Q}_{\mathrm{A}} = \eta - \xi_{\mathrm{S}}\hat{Q}_{\mathrm{R}}, \tag{24}$$

$$\hat{Q}_{\mathrm{B}} = (1-\eta) - (1-\xi_{\mathrm{S}})\hat{Q}_{\mathrm{R}}, \tag{25}$$

where $\hat{Q}_\alpha = Q_\alpha/\Gamma_{\alpha 0}$. By using the first moment closure for the conditional mean reaction rate, the conditional mean production rate of $\hat{Q}_{\mathrm{R}}$ by the chem-

ical reaction can be written as

$$\langle \hat{W}_{\mathrm{R}} \mid \eta \rangle = Da \hat{Q}_{\mathrm{A}} \hat{Q}_{\mathrm{B}} \tag{26}$$

$$= Da[\eta - \xi_{\mathrm{S}} \hat{Q}_{\mathrm{R}}][(1-\eta) - (1-\xi_{\mathrm{S}}) \hat{Q}_{\mathrm{R}}], \tag{27}$$

where $\hat{W}_{\mathrm{R}}$ is the normalized production and is given by $\hat{W}_{\mathrm{R}} = W_{\mathrm{R}} d / \{(U_{\mathrm{J}} - U_{\mathrm{M}}) \Gamma_{\mathrm{R0}}\}$. The mixture fraction value at which $\langle \hat{W}_{\mathrm{R}} \mid \eta \rangle$ has a peak is obtained from $\partial \langle \hat{W}_{\mathrm{R}} \mid \eta \rangle / \partial \eta = 0$. From Eq. (27), $\partial \langle \hat{W}_{\mathrm{R}} \mid \eta \rangle / \partial \eta$ can be written as

$$\frac{\partial \langle \hat{W}_{\mathrm{R}} \mid \eta \rangle}{\partial \eta} = Da \left\{ (1-2\eta) - (1-2\xi_{\mathrm{S}}) \hat{Q}_{\mathrm{R}} - \left[\xi_{\mathrm{S}} + (1-2\xi_{\mathrm{S}}) \eta - 2\xi_{\mathrm{S}} (1-\xi_{\mathrm{S}}) \hat{Q}_{\mathrm{R}} \right] \frac{\partial \hat{Q}_{\mathrm{R}}}{\partial \eta} \right\}. \tag{28}$$

Assuming that the conditional mean concentration of product R reaches a peak on the condition that $\langle \hat{W}_{\mathrm{R}} \mid \eta \rangle$ has the peak value, we can obtain the following equation by substituting $\partial \hat{Q}_{\mathrm{R}} / \partial \eta = 0$ and $\partial \langle \hat{W}_{\mathrm{R}} \mid \eta \rangle / \partial \eta = 0$ in Eq. (28):

$$(1-2\eta) - (1-2\xi_{\mathrm{S}}) \hat{Q}_{\mathrm{R}} = 0. \tag{29}$$

Then, the peak value of $\hat{Q}_{\mathrm{R}}$ can be related to the mixture fraction by

$$\hat{Q}_{\mathrm{R}} = \frac{1-2\eta}{1-2\xi_{\mathrm{S}}}. \tag{30}$$

By substituting Eq. (30) in Eqs. (24) and (25), the conditional mean concentration of reactants A and B corresponding to Eq. (29) can be obtained as

$$\hat{Q}_{\mathrm{A}} = \hat{Q}_{\mathrm{B}} = \frac{\eta - \xi_{\mathrm{S}}}{1-2\xi_{\mathrm{S}}}. \tag{31}$$

Figs. 5(a) and (b) show $\hat{Q}_{\mathrm{A}}$ and $\hat{Q}_{\mathrm{B}}$ given by Eq. (31) and $\hat{Q}_{\mathrm{R}}$ given by Eq. (30) (solid lines). From Fig. 5(b), it is found that $\hat{Q}_{\mathrm{R}}$ has a peak on the

line given by Eq. (30). Additionally, Fig. 5(a) shows that $\hat{Q}_{\rm A}$ and $\hat{Q}_{\rm B}$ also satisfy $\hat{Q}_{\rm A} = \hat{Q}_{\rm B}$ on the line given by Eq. (31). Therefore, the assumption that $\hat{Q}_{\rm R}$ reaches its peak on the condition that $\langle \hat{W}_{\rm R} \mid \eta \rangle$ has a peak is valid on the jet centreline.

Figs. 6 and 7 show the cross-streamwise variations of $\hat{Q}_\alpha$ at $x/d = 10$ and 40, the conditional mean concentrations for the frozen and equilibrium limits and the lines given by Eqs. (30) and (31). At $x/d = 10$, $Q_{\rm A}$ and $Q_{\rm B}$ decrease, and $Q_{\rm R}$ increases from $y/b_\xi = 0$ towards $y/b_\xi = 1$, although the conditional mean concentrations are independent of the cross-streamwise position beyond $y/b_\xi = 1$. At $x/d = 10$, $Q_{\rm R}$ at $y/b_\xi = 1$ and 1.5 has a peak at η smaller than expected from Eq. (30). Therefore, near the edge of the jet flow, the condition that the conditional mean reaction rate has a peak is not consistent with the condition that the conditional mean concentration of product R has a peak. Fig. 7 shows that the conditional mean concentrations are independent of the cross-streamwise position in the downstream region.

The covariance of conditional concentration fluctuations γ''_α is defined by $G_{\alpha\beta} \equiv \langle \gamma''_\alpha \gamma''_\beta \mid \eta \rangle$, where $\alpha, \beta = {\rm A, B}$ or R. For the second-order chemical reaction ${\rm A} + {\rm B} \rightarrow {\rm R}$, the magnitude of $G_{\alpha\beta}$ does not depend on reactive species α and β. For example, $G_{\rm AA} = G_{\rm RR}$ can be derived by using Eq. (7):

$$
\begin{aligned}
\langle \gamma''^2_{\rm A} \mid \eta \rangle &= \langle \mathit{\Gamma}^2_{\rm A} \mid \eta \rangle - \langle \mathit{\Gamma}_{\rm A} \mid \eta \rangle^2 \\
&= \langle (\xi \mathit{\Gamma}_{\rm A0} - \mathit{\Gamma}_{\rm R})^2 \mid \eta \rangle - \langle \xi \mathit{\Gamma}_{\rm A0} - \mathit{\Gamma}_{\rm R} \mid \eta \rangle^2 \\
&= (\mathit{\Gamma}^2_{\rm A0}\eta^2 - 2\mathit{\Gamma}_{\rm A0}\eta \langle \mathit{\Gamma}_{\rm R} \mid \eta \rangle + \langle \mathit{\Gamma}^2_{\rm R} \mid \eta \rangle) \\
&\qquad -(\mathit{\Gamma}^2_{\rm A0}\eta^2 - 2\mathit{\Gamma}_{\rm A0}\eta \langle \mathit{\Gamma}_{\rm R} \mid \eta \rangle + \langle \mathit{\Gamma}_{\rm R} \mid \eta \rangle^2) \qquad (32) \\
&= \langle \mathit{\Gamma}^2_{\rm R} \mid \eta \rangle - \langle \mathit{\Gamma}_{\rm R} \mid \eta \rangle^2
\end{aligned}
$$

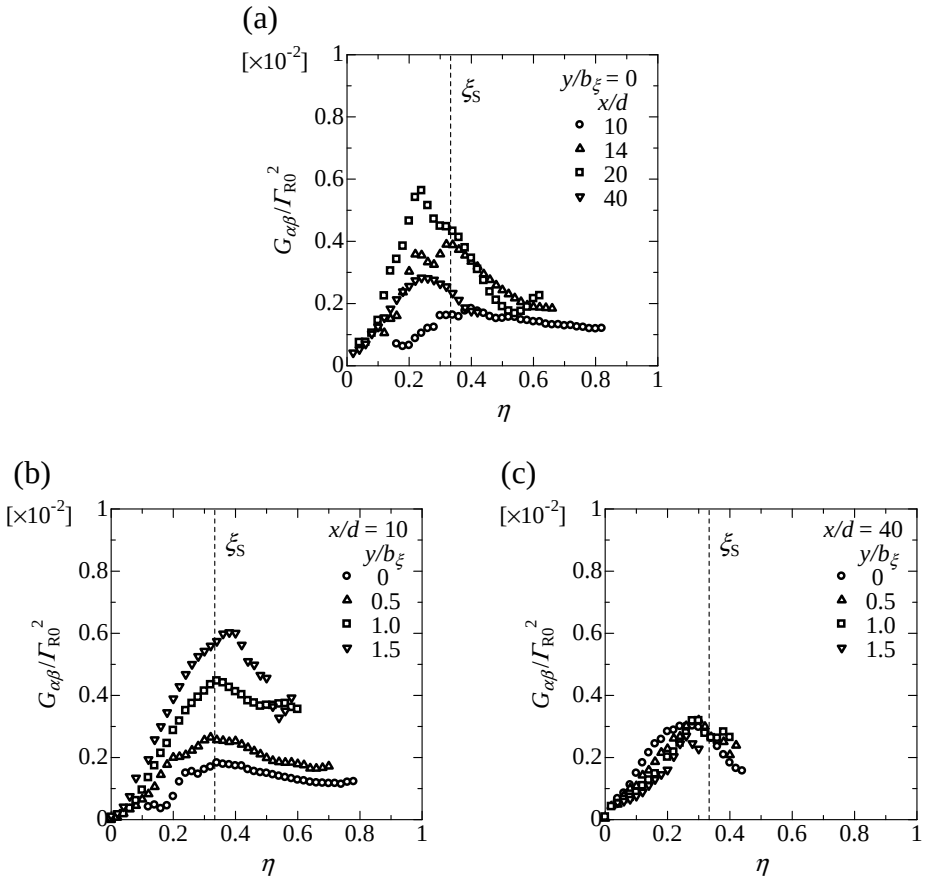

Figure 8: Covariance of conditional concentration fluctuations. (a) Streamwise variation on the jet centreline. (b) Cross-streamwise variation at $x/d = 10$. (c) Cross-streamwise variation at $x/d = 40$.

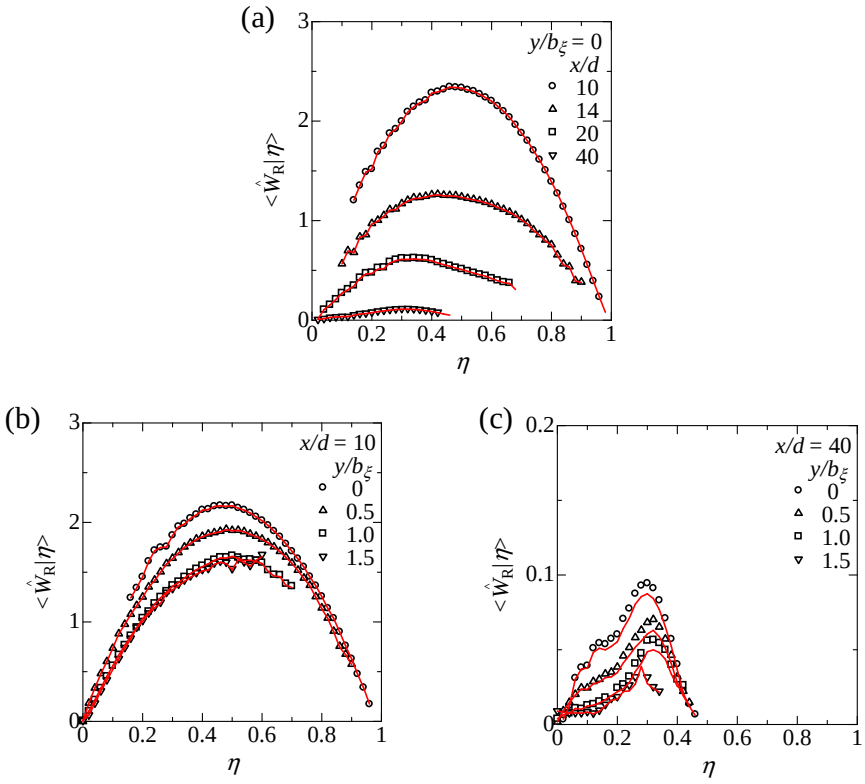

Figure 9: Conditional mean reaction rate. Solid line: Eq. (26). (a) Streamwise variation on the jet centreline. (b) Cross-streamwise variation at $x/d = 10$. (c) Cross-streamwise variation at $x/d = 40$.

$$= \langle \gamma''^2_{\mathrm{R}} \mid \eta \rangle.$$

Similarly, $|G_{\alpha\beta}| = G_{\mathrm{RR}}$ can be derived for $\alpha, \beta = \mathrm{A}, \mathrm{B}$ or R. Figs. 8(a), (b) and (c) show the streamwise variation of $G_{\alpha\beta}/\Gamma^2_{\mathrm{R}0}$ on the jet centreline and the cross-streamwise variations of $G_{\alpha\beta}/\Gamma^2_{\mathrm{R}0}$ at $x/d = 10$ and 40. In Fig. 8, $\eta = \xi_{\mathrm{S}}$ is shown by the broken line. Previous measurements of $G_{\alpha\beta}$ conducted by Li and Bilger [26] clarified that $G_{\alpha\beta}$ has a peak at $\eta \approx \xi_{\mathrm{S}}$ in the reactive scalar mixing layer. This tendency can be seen in our measurement results. At $x/d = 10$ and 14 on the jet centreline, $G_{\alpha\beta}$ has a peak at $\eta \approx \xi_{\mathrm{S}}$, whereas further downstream on the jet centreline, $G_{\alpha\beta}$ has a peak at η slightly smaller than ξ_{S}. From Fig. 8(a), it is found that the peak value of $G_{\alpha\beta}$ on the jet centreline increases from $x/d = 10$ towards $x/d = 20$ and decreases further downstream. $G_{\alpha\beta}$ increases in the cross-streamwise direction at $x/d = 10$, as shown in Fig. 8(b). However, Fig. 8(c) shows that $G_{\alpha\beta}$ for $\eta \leq 0.25$ decreases in the cross-streamwise direction at $x/d = 40$.

In the CMC method, the first moment closure given by Eq. (26) is widely used to close the conditional mean reaction rate. Figs. 9(a), (b) and (c) show the streamwise variation of $\langle \hat{W}_{\mathrm{R}} \mid \eta \rangle$ on the jet centreline and the cross-streamwise variations of $\langle \hat{W}_{\mathrm{R}} \mid \eta \rangle$ at $x/d = 10$ and 40. Fig. 9 also shows $\langle \hat{W}_{\mathrm{R}} \mid \eta \rangle$ predicted by Eq. (26). From Fig. 9, it is found that the conditional mean reaction rate is well predicted by using the first moment closure. $\langle \hat{W}_{\mathrm{R}} \mid \eta \rangle$ is large at $x/d = 10$, and it decreases in the downstream direction because the concentrations of reactants become small, as shown in Fig. 5(a). At $x/d = 10$, $\langle \hat{W}_{\mathrm{R}} \mid \eta \rangle$ is large on the jet centreline, and it decreases in the cross-streamwise direction from $y/b_\xi = 0$ towards $y/b_\xi = 1$, whereas $\langle \hat{W}_{\mathrm{R}} \mid \eta \rangle$ at $x/d = 10$ is independent of the cross-streamwise position beyond $y/b_\xi = 1$.

At $x/d = 40$, $\langle \hat{W}_{\mathrm{R}} \mid \eta \rangle$ is very small compared with that in the upstream region. However, the change in $G_{\alpha\beta}$ in the downstream direction is smaller than that in $\langle \hat{W}_{\mathrm{R}} \mid \eta \rangle$. Therefore, the contribution of $G_{\alpha\beta}$ to $\langle \hat{W}_{\mathrm{R}} \mid \eta \rangle$ is expected to be important in the downstream direction. Figs. 9 and 8 show that the first moment closure for the conditional mean reaction rate is valid for the second-order isothermal reaction in the planar liquid jet. The intensities of conditional fluctuations depend on the flow configuration and on the nature of chemical reactions [19]. Therefore, for different reactions, such as reactions with significant heat release, or in different flows, this model for the conditional mean reaction rate may not be accurate.

The conditional mean concentrations and the conditional mean reaction rate are independent of the cross-streamwise position away from the jet exit (e.g., the edge of the jet flow or the downstream region). It has been shown that the conditional mean concentrations are independent of the cross-streamwise position in the reactive scalar mixing layer [18] and in the reactive plume in grid turbulence [27]. This characteristic can be used to simplify the CMC equation (Eq. (2)). Indeed, the assumption that the conditional mean concentrations do not depend on the cross-streamwise direction is often used in the CMC method (e.g., [27, 53, 54]). However, this assumption is not valid near the jet exit in the planar liquid jet investigated in this study. Because the conditional mean reaction rate is large near the jet exit as shown in Figs. 9(a) and (b), it is important to accurately predict the conditional mean concentrations of reactive species near the jet exit. Therefore, the assumption of cross-streamwise direction independence of conditional statistics might lead to errors in the prediction of conditional mean concentration.

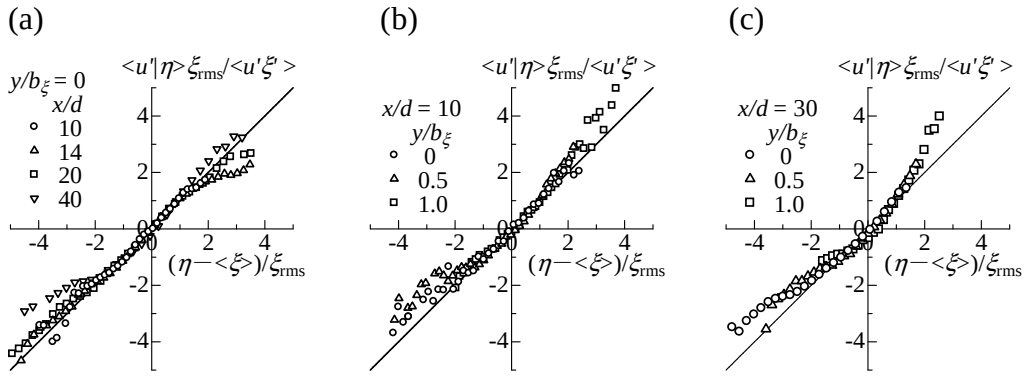

Figure 10: Conditional mean streamwise velocity. Solid line: Eq. (33). (a) Streamwise variation on the jet centreline. (b) Cross-streamwise variation at $x/d = 10$. (c) Cross-streamwise variation at $x/d = 30$.

4.4. Conditional mean velocity

The conditional mean velocity $\langle U_i \mid \eta \rangle$ appears in the CMC equation in an unclosed form, and it has to be modelled to solve the CMC equation. When the joint probability density function of velocity fluctuation $u_i' \equiv U_i - \langle U_i \rangle$ and mixture fraction fluctuation $\xi' \equiv \xi - \langle \xi \rangle$ is represented by a joint Gaussian function, the conditional mean velocity is given by the linear model [55]

$$\langle u_i' \mid \eta \rangle = \langle U_i \mid \eta \rangle - \langle U_i \rangle = \frac{\langle u_i' \xi' \rangle}{\xi_{\rm rms}^2} (\eta - \langle \xi \rangle). \tag{33}$$

Here, $\xi_{\rm rms}$ is the rms value of the mixture fraction fluctuation. In this model, the velocity fluctuation is assumed to be linear to the mixture fraction fluctuation. Figs. 10(a), (b) and (c) show the streamwise variation of the conditional mean streamwise velocity $\langle u' \mid \eta \rangle \xi_{\rm rms} / \langle u' \xi' \rangle$ on the jet centreline and the cross-streamwise variations of $\langle u' \mid \eta \rangle \xi_{\rm rms} / \langle u' \xi' \rangle$ at $x/d = 10$ and 30 versus $(\eta - \langle \xi \rangle)/\xi_{\rm rms}$. In Fig. 10, Eq. (33) is shown by the solid

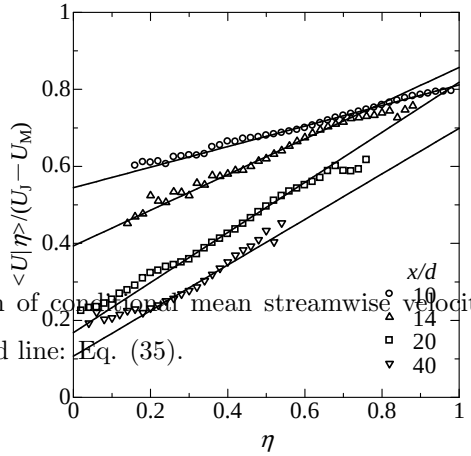

Figure 11: Comparison of conditional mean streamwise velocity with the linear model given by Eq. (35). Solid line: Eq. (35).

line. Because of the positive correlation between the streamwise velocity and mixture fraction fluctuations, large u' corresponds to large η', and small u' corresponds to small η'. Eq. (33) is valid on the jet centreline for $|\eta - \langle\xi\rangle|/\xi_{\rm rms} < 2$, whereas $\langle u' \mid \eta\rangle$ is different from Eq. (33) when the mixture fraction fluctuation is large in magnitude. Fig. 10(b) shows that Eq. (33) is also valid for $|\eta - \langle\xi\rangle|/\xi_{\rm rms} < 2$ at $x/d = 10$. However, at $x/d = 30$ (Fig. 10(c)), the difference between $\langle u' \mid \eta\rangle$ and Eq. (33) becomes large for $-2 \leq (\eta - \langle\xi\rangle)/\xi_{\rm rms} \leq -1$ in the cross-streamwise direction because the joint probability density function of u' and ξ' is far from Gaussian near the edge of the jet flow because of intermittency. These differences between the measured $\langle u' \mid \eta\rangle$ and Eq. (33) for large $|\eta'|$ can be seen in the previous measurements of conditional mean velocity conducted by Li and Bilger [56] and Feng et al [57].

Figure 12: Streamwise variation of $\beta = \langle \hat{W}_{\mathrm{R}} \mid \eta \rangle / Da \hat{Q}_{\mathrm{R}}$ on the jet centreline.

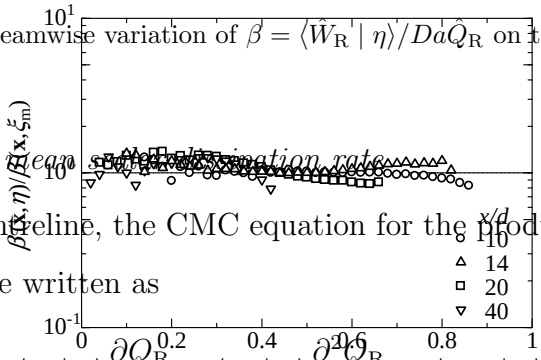

4.5. Conditional mean scalar dissipation rate

On the jet centreline, the CMC equation for the product R in the steady scalar field can be written as

$$\langle U \mid \eta \rangle \frac{\partial Q_{\mathrm{R}}}{\partial x} - \langle N \mid \eta \rangle \frac{\partial^2 Q_{\mathrm{R}}}{\partial \eta^2} = \langle W_{\mathrm{R}} \mid \eta \rangle. \tag{34}$$

In this study, the budget of Eq. (34) is used to calculate the conditional mean scalar dissipation rate $\langle N \mid \eta \rangle$ on the jet centreline. The CMC equation is a model equation that is valid under some assumptions [19]. However, because several numerical simulations using the CMC method have succeeded in accurately predicting the conditional statistics in reactive jet flows [53, 54], the CMC equation is expected to be valid in a planar liquid jet with a chemical reaction. We use some models to estimate the conditional statistics for $0 \leq \eta \leq 1$.

As shown in Fig. 10, Eq. (33) is valid on the jet centreline. The condi-

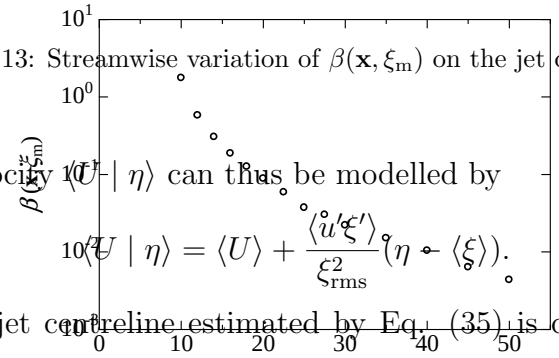

Figure 13: Streamwise variation of $\beta(\mathbf{x}, \xi_{\rm m})$ on the jet centreline.

tional mean velocity $\langle U \mid \eta \rangle$ can thus be modelled by

$$\langle U \mid \eta \rangle = \langle U \rangle + \frac{\langle u'\xi' \rangle}{\xi_{\rm rms}^2}(\eta - \langle \xi \rangle). \tag{35}$$

$\langle U \mid \eta \rangle$ on the jet centreline estimated by Eq. (35) is compared with the measurement results in Fig. 11. It is found that $\langle U \mid \eta \rangle$ is well approximated by Eq. (35).

To calculate $\partial Q_{\rm R}/\partial x$ and $\partial^2 Q_{\rm R}/\partial \eta^2$ for $0 \leq \eta \leq 1$, $Q_{\rm R}$ is modelled by using the assumption that the normalized conditional mean concentration of product R is proportional to the normalized conditional mean reaction rate. We introduce $\beta(\mathbf{x}, \eta)$, a function that satisfies

$$\langle \hat{W}_{\rm R} \mid \eta \rangle = Da\beta \hat{Q}_{\rm R}. \tag{36}$$

Solving the equation obtained by substituting $\langle \hat{W}_{\rm R} \mid \eta \rangle = Da\beta\hat{Q}_{\rm R}$ in Eq. (27) by considering $0 \leq \hat{Q}_{\rm R} \leq 1$ yields the following expression for the conditional mean concentration of product R:

$$\hat{Q}_{\rm R} = \frac{1}{2\xi_{\rm S}(1-\xi_{\rm S})}\Big[\beta + \xi_{\rm S}(1-\eta) + \eta(1-\xi_{\rm S})$$

$$- \sqrt{[\beta + \xi_{\rm S}(1-\eta) + \eta(1-\xi_{\rm S})]^2 - 4\xi_{\rm S}(1-\xi_{\rm S})\eta(1-\eta)}\Big]. \quad (37)$$

Fig. 12 shows the measurement results of $\beta(\mathbf{x},\eta) = \langle \hat{W}_{\rm R} \mid \eta \rangle / (Da\hat{Q}_{\rm R})$ on the jet centreline normalized by $\beta(\mathbf{x},\xi_{\rm m})$, where $\xi_{\rm m}$ is the mixture fraction value at which $Q_{\rm R}$ reaches a peak. From Fig. 12, it is found that β is almost independent of η. Therefore, assuming $\beta(\mathbf{x},\eta)$ is independent of η and is nearly equal to the measured $\beta(\mathbf{x},\xi_{\rm m})$, we can estimate the conditional mean concentration of product R for $0 \le \eta \le 1$ from Eq. (37). Then, the conditional mean concentrations of reactants A and B can be obtained by substituting Eq. (37) into Eqs. (24) and (25).

Fig. 13 shows the streamwise variation of $\beta(\mathbf{x},\xi_{\rm m})$ on the jet centreline. The conditional mean reaction rate $\langle \hat{W}_{\rm R} \mid \eta \rangle$ is large in the upstream region and decreases in the downstream direction because reactants A and B are consumed by the chemical reaction, whereas the conditional mean concentration of product R, $\hat{Q}_{\rm R}$, increases in the downstream direction. Therefore, $\beta(\mathbf{x},\xi_{\rm m})$ decreases in the downstream direction.

Fig. 14 shows the measured conditional mean concentrations and the conditional mean concentrations estimated from Eq. (37). The conditional mean concentrations estimated from Eq. (37) agree well with the measured conditional mean concentrations. Therefore, Eq. (37) can be used to calculate $\partial Q_{\rm R}/\partial x$, $\partial^2 Q_{\rm R}/\partial \eta^2$ and $\langle \hat{W}_{\rm R} \mid \eta \rangle$.

The conditional mean reaction rate on the jet centreline is well approximated by using the first moment closure, as shown in Fig. 9. Fig. 15 shows $\langle \hat{W}_{\rm R} \mid \eta \rangle = Da\hat{Q}_{\rm A}\hat{Q}_{\rm B}$ estimated by using Eq. (37). $\langle \hat{W}_{\rm R} \mid \eta \rangle$ decreases in the downstream direction because the conditional mean concentrations of reactants A and B decrease owing to the chemical reaction. At $x/d = 10$,

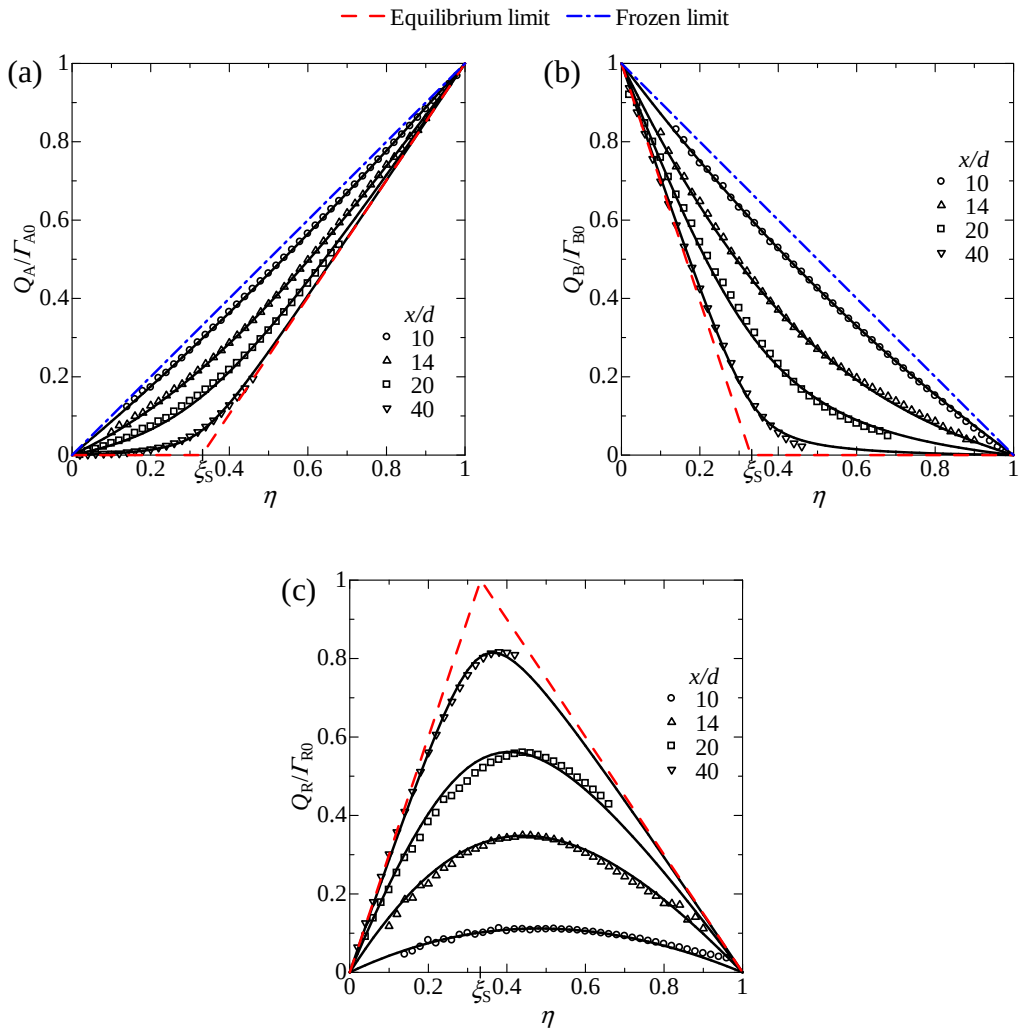

Figure 14: Comparison of conditional mean concentration with Eq. (37). Solid line: Eq. (37). (a) Reactant A. (b) Reactant B. (c) Product R.

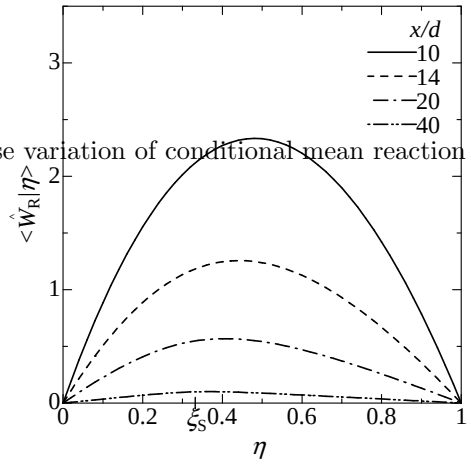

Figure 15: Streamwise variation of conditional mean reaction rate on the jet centreline.

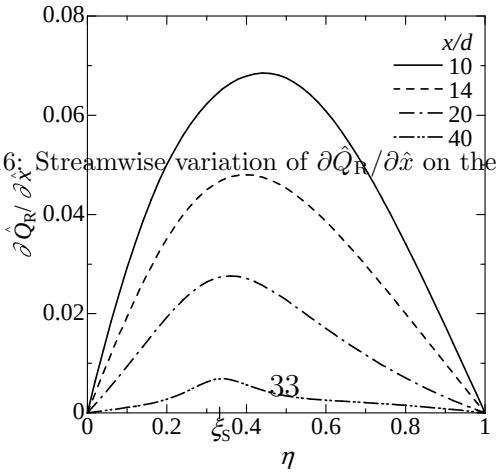

Figure 16: Streamwise variation of $\partial \hat{Q}_R / \partial \hat{x}$ on the jet centreline.

$\langle \hat{W}_{\mathrm{R}} \mid \eta \rangle$ has a peak at $\eta \approx 0.5$. In the downstream direction, the mixture fraction value at which $\langle \hat{W}_{\mathrm{R}} \mid \eta \rangle$ reaches a peak decreases and approaches ξ_{S}.

Fig. 16 shows the streamwise variation of $\partial \hat{Q}_{\mathrm{R}}/\partial \hat{x}$ on the jet centreline. Here, $\hat{x} \equiv x/d$. Because the chemical reaction proceeds in the downstream direction, the concentration of product R increases in the downstream direction, and $\partial \hat{Q}_{\mathrm{R}}/\partial \hat{x} > 0$. Comparison between $\langle \hat{W}_{\mathrm{R}} \mid \eta \rangle$ and $\partial \hat{Q}_{\mathrm{R}}/\partial \hat{x}$ (Figs. 15 and 16) indicates that $\partial \hat{Q}_{\mathrm{R}}/\partial \hat{x}$ becomes large on the condition that $\langle \hat{W}_{\mathrm{R}} \mid \eta \rangle$ becomes large because the large $\partial \hat{Q}_{\mathrm{R}}/\partial \hat{x}$ can be related to the large production of product R by the chemical reaction.

Fig. 17 shows the streamwise variation of $\partial^2 \hat{Q}_{\mathrm{R}}/\partial \eta^2$ on the jet centreline. $\partial^2 \hat{Q}_{\mathrm{R}}/\partial \eta^2$ is negative, and it changes significantly with the streamwise position on the jet centreline. $\partial^2 \hat{Q}_{\mathrm{R}}/\partial \eta^2$ is almost independent of η at $x/d = 10$, whereas $\partial^2 \hat{Q}_{\mathrm{R}}/\partial \eta^2$ has a negative peak at $\eta \approx \xi_{\mathrm{S}}$ in the downstream region. In the downstream direction, the conditional mean concentrations approach the equilibrium limit values, for which the conditional mean concentrations linearly change with mixture fraction except for $\eta = \xi_{\mathrm{S}}$. At $\eta = \xi_{\mathrm{S}}$, $\partial \hat{Q}_{\alpha}/\partial \eta$ for the equilibrium limit discontinuously changes with η. Therefore, in the downstream region, $\partial^2 \hat{Q}_{\mathrm{R}}/\partial \eta^2$ is large in magnitude at $\eta \approx \xi_{\mathrm{S}}$ because the first derivative $\partial \hat{Q}_{\mathrm{R}}/\partial \eta$ changes significantly at $\eta \approx \xi_{\mathrm{S}}$, as shown in Fig. 14. In contrast, $\partial^2 \hat{Q}_{\mathrm{R}}/\partial \eta^2$ in the downstream region is small at η much smaller or larger than ξ_{S}, for which $\hat{Q}_{\mathrm{R}}$ is almost linear to the mixture fraction.

The conditional scalar dissipation rate $\langle N \mid \eta \rangle$ on the jet centreline can be obtained from the budget of Eq. (34) by using the model equations (Eqs. (27), (35) and (37)). Fig. 18 shows the streamwise variation of $\langle \hat{N} \mid \eta \rangle$ on the jet centreline. Here, $\hat{N} \equiv Nd/(U_{\mathrm{J}} - U_{\mathrm{M}})$. Fig. 18(a) shows $\langle N \mid \eta \rangle$

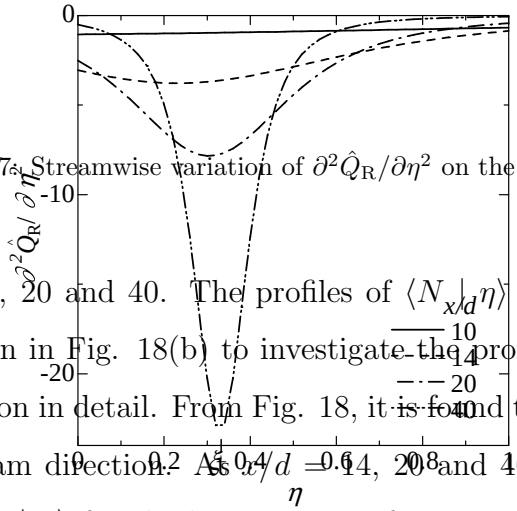

Figure 17: Streamwise variation of $\partial^2\hat{Q}_{\mathrm{R}}/\partial\eta^2$ on the jet centreline.

at $x/d = 10$, 14, 20 and 40. The profiles of $\langle N \mid \eta \rangle$ at $x/d = 14$, 20 and 40 are also shown in Fig. 18(b) to investigate the profiles of $\langle N \mid \eta \rangle$ in the downstream region in detail. From Fig. 18, it is found that $\langle N \mid \eta \rangle$ decreases in the downstream direction. As $x/d = 14$, 20 and 40, $\langle N \mid \eta \rangle$ is large at $\eta \approx 0.8$, and $\langle N \mid \eta \rangle$ for the large mixture fraction is larger than that for the small mixture fraction. The previous measurements of conditional scalar dissipation rate conducted by Kailasnath et al. [40] also show that $\langle N \mid \eta \rangle$ is large for the large mixture fraction. In the upstream region, $\langle N \mid \eta \rangle$ has a single peak. However, at $x/d = 40$, $\langle N \mid \eta \rangle$ has a local minimum value, and it has two peaks at $\eta \approx 0.1$ and 0.8. The peak value of $\langle N \mid \eta \rangle$ at $\eta \approx 0.1$ is much smaller than that at $\eta \approx 0.8$. These two peaks of conditional scalar dissipation rate were also seen in Kailasnath et al. [40] and Kim and Pitsch [58].

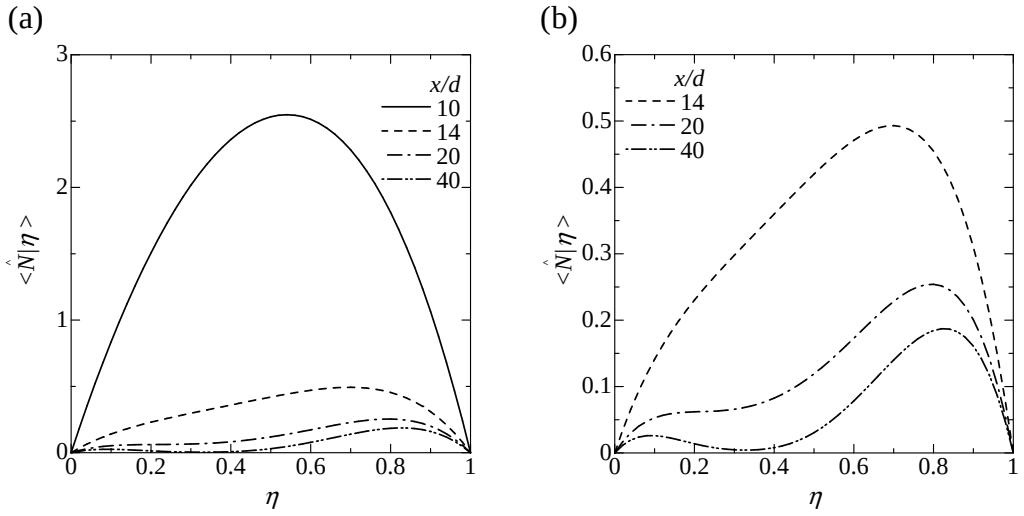

Figure 18: Conditional scalar dissipation rate on the jet centreline. (a) Conditional scalar dissipation rate in the upstream region. (b) Conditional scalar dissipation rate in the downstream region.

The mean scalar dissipation rate $\langle N \rangle$ can be calculated from the conditional scalar dissipation rate and the probability density function of the mixture fraction:

$$\langle N \rangle = \int_0^1 \langle N \mid \eta \rangle p_\xi(\eta) d\eta. \tag{38}$$

Fig. 19 shows the streamwise decay of the mean scalar dissipation rate on the jet centreline. In Fig. 19, x^* is the streamwise position from the virtual origin x_0. x_0 is determined from the streamwise variation of the mean mixture fraction on the jet centreline, and $x_0 = 4.3d$. Bilger [31] derived the scaling law of $\langle N \rangle \propto (x^*/d)^{-2.5}$ on the jet centreline of a planar jet by assuming self-similarity of jet flow and neglecting a few terms in the transport equations for the mixture fraction and the mixture fraction variance. However, Peters and Williams [59] derived $\langle N \rangle \propto (x^*/d)^{-3}$ on the jet centreline of a planar jet by relating the decay of the mean scalar dissipation rate to the decay of the mean dissipation rate of turbulent kinetic energy. In this study, $\langle N \rangle \propto (x^*/d)^{-2.9}$ can be obtained by applying the least-squares method to $\langle N \rangle$ in $x/d \geq 20$ where the cross-streamwise profiles of the mean mixture fraction and the mixture fraction variance show self-similarity [44]. Our result is close to the scaling law $\langle N \rangle \propto (x^*/d)^{-3}$ of the scalar dissipation rate of Peters and Williams [59], rather than $\langle N \rangle \propto (x^*/d)^{-2.5}$ derived by Bilger [31].

Su and Clemens [37] measured the scalar dissipation rate in a planar jet, and their measurement showed that the mean scalar dissipation rate on the jet centreline is proportional to $(x/d)^{-1.4}$, which is different from the results of both Peters and Williams [59] and Bilger [31]. Bilger [31] pointed out that this difference is caused by the spatial resolution in Su and Clemens [37] being inadequate for measuring the scalar dissipation rate. Su et al.

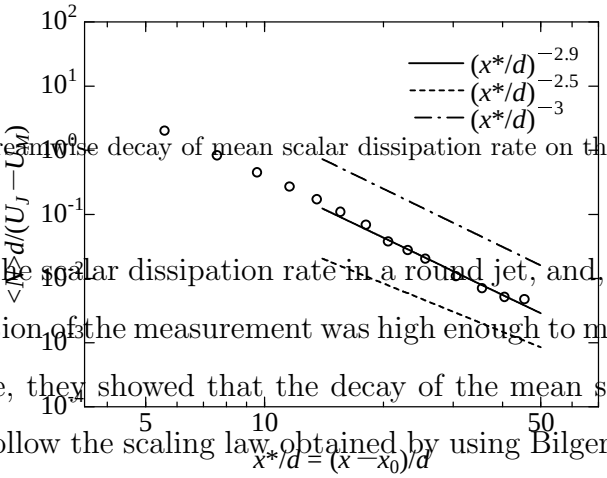

Figure 19: Streamwise decay of mean scalar dissipation rate on the jet centreline.

[39] measured the scalar dissipation rate in a round jet, and, after confirming that the resolution of the measurement was high enough to measure the scalar dissipation rate, they showed that the decay of the mean scalar dissipation rate does not follow the scaling law obtained by using Bilger's assumption of self-similar profiles of mean scalar dissipation rate [31]. They suggested that the non-self-similar profiles of mean scalar dissipation rate are responsible for the difference between the measured mean scalar dissipation rate and the scaling law of Bilger [31]. In this paper, the conditional mean dissipation rate is calculated from the conditional mean concentration and the conditional mean velocity, the measurements of which are not as difficult to perform as those for the scalar dissipation rate. Because the cross-streamwise profiles of the mean scalar dissipation rate are not available, the assumption of self-similar profiles of the mean scalar dissipation rate used by Bilger [31] cannot be checked in this study. As suggested by Su et al. [39], the mean scalar

dissipation rate might not decrease according to the scaling law obtained by Bilger [31] owing to the non-self-similar profiles of the mean scalar dissipation rate in our measurement region.

5. Conclusion

Conditional statistics, conditioned on mixture fraction, were investigated in a planar liquid jet with the second-order isothermal chemical reaction $A + B \rightarrow R$. Reactants A and B were contained in the jet and ambient flows, respectively, and were supplied into the test section under the non-premixed condition. Simultaneous measurements of streamwise velocity and concentrations of reactive species were conducted by using an I-type hot-film probe and an optical fibre probe based on light absorption spectrometry.

The conditional mean concentrations of reactive species and the conditional mean reaction rate both change with the cross-streamwise position near the jet exit, whereas they are independent of the cross-streamwise position near the edge of the jet flow and in the downstream region. The conditional mean concentrations are close to the frozen limit values near the jet exit. In the downstream direction, the conditional mean concentrations approach the equilibrium limit values because of the progress of the chemical reaction. On the jet centreline, the conditional mean reaction rate has a peak on the condition that the conditional mean concentration of product R has a peak and the conditional mean concentrations of reactants A and B are equal to each other.

The covariance of conditional concentration fluctuations in the upstream region has a peak for a mixture fraction value nearly equal to its stoichiomet-

ric value. The contribution of the covariance of concentration fluctuations to the conditional mean reaction rate can be important in the downstream region. However, the covariance of concentration fluctuations is small enough that the first moment closure model for the conditional mean reaction rate is valid.

The conditional mean streamwise velocity on the jet centreline is linear to the mixture fraction for small mixture fraction fluctuations, whereas the linear model for the conditional mean velocity is not valid for large mixture fraction fluctuations. Near the edge of the jet flow in the downstream region, the conditional mean velocity cannot be accurately estimated by using a linear model because of intermittency.

The conditional scalar dissipation rate on the jet centreline was calculated from the budget of the CMC equation. The conditional scalar dissipation rate becomes small in the downstream direction. In the upstream region, the conditional scalar dissipation rate has one peak. However, in the downstream region, the conditional scalar dissipation rate has two peaks (for large and small mixture fraction values). The peak value for the small mixture fraction is much smaller than that for the large mixture fraction.

The conventional mean scalar dissipation rate was calculated from the probability density function of the mixture fraction and the conditional scalar dissipation rate. The mean scalar dissipation rate decreases in the downstream direction as $(x^*/d)^{-2.9}$, which is almost the same as predicted by Peters and Williams [59].

5.0.1. Acknowledgment

This work was supported by JSPS KAKENHI Grant Number 25002531

and MEXT KAKENHI Grant Numbers 25289030, 25289031 and 25630052.

References

[1] J. C. Hill, Homogeneous turbulent mixing with chemical reaction, Annu. Rev. Fluid Mech. 8 (1976) 135–161.

[2] D. Veynante, L. Vervisch, Turbulent combustion modeling, Prog. Energy Combust. Sci. 28 (3) (2002) 193–266.

[3] P. A. McMurtry, W. H. Jou, J. Riley, R. W. Metcalfe, Direct numerical simulations of a reacting mixing layer with chemical heat release, AIAA J. 24 (6) (1986) 962–970.

[4] R. S. Miller, C. K. Madnia, P. Givi, Structure of a turbulent reacting mixing layer, Combust. Sci. Tech. 99 (1-3) (1994) 1–36.

[5] L. Vervisch, T. Poinsot, Direct numerical simulation of non-premixed turbulent flames, Annu. Rev. Fluid Mech. 30 (1) (1998) 655–691.

[6] S. M. de Bruyn Kops, J. J. Riley, G. Kosaly, Direct numerical simulation of reacting scalar mixing layers, Phys. Fluids 13 (2001) 1450.

[7] A. Fabregat, J. Pallarès, I. Cuesta, F. X. Grau, Numerical simulations of a second-order chemical reaction in a plane turbulent channel flow, Int. J. Heat Mass Transfer 53 (19) (2010) 4248–4263.

[8] Z. Pouransari, G. Brethouwer, A. V. Johansson, Direct numerical simulation of an isothermal reacting turbulent wall-jet, Phys. Fluids 23 (2011) 085104.

[9] D. P. Combest, P. A. Ramachandran, M. P. Dudukovic, On the gradient diffusion hypothesis and passive scalar transport in turbulent flows, Ind. Eng. Chem. Res. 50 (15) (2011) 8817–8823.

[10] D. M. Wang, J. M. Tarbell, Closure models for turbulent reacting flows with a nonhomogeneous concentration field, Chem. Eng. Sci. 48 (23) (1993) 3907–3920.

[11] H. L. Toor, Turbulent mixing of two species with and without chemical reactions, Ind. Eng. Chem. Fundam. 8 (4) (1969) 655–659.

[12] G. K. Patterson, Application of turbulence fundamentals to reactor modelling and scaleup, Chem. Eng. Commun. 8 (1-3) (1981) 25–52.

[13] A. Dutta, J. M. Tarbell, Closure models for turbulent reacting flows, AIChE J. 35 (12) (1989) 2013–2027.

[14] R. W. Bilger, L. R. Saetran, L. V. Krishnamoorthy, Reaction in a scalar mixing layer, J. Fluid Mech. 233 (1991) 211–242.

[15] H. L. Toor, Effect of chemical reactions on turbulent diffusivities, AIChE J. 39 (10) (1993) 1603–1610.

[16] S. Komori, K. Nagata, T. Kanzaki, Y. Murakami, Measurements of mass flux in a turbulent liquid flow with a chemical reaction, AIChE J. 39 (10) (1993) 1611–1620.

[17] T. Watanabe, Y. Sakai, K. Nagata, O. Terashima, Turbulent Schmidt number and eddy diffusivity change with a chemical reaction, J. Fluid Mech. 754 (2014) 98–121.

[18] R. W. Bilger, Conditional moment closure for turbulent reacting flow, Phys. Fluids A 5 (1993) 436.

[19] A. Y. Klimenko, R. W. Bilger, Conditional moment closure for turbulent combustion, Prog. Energy Combust. Sci. 25 (6) (1999) 595–687.

[20] A. R. Masri, R. W. Dibble, R. S. Barlow, The structure of turbulent nonpremixed flames of methanol over a range of mixing rates, Combust. Flame 89 (2) (1992) 167–185.

[21] A. Y. Klimenko, Multicomponent diffusion of various admixtures in turbulent flow, Fluid Dyn. 25 (3) (1990) 327–334.

[22] S. Komori, T. Kanzaki, Y. Murakami, Concentration correlation in a turbulent mixing layer with chemical reactions, J. Chem. Eng. Jpn. 27 (6) (1994) 742–748.

[23] A. D. Chornyi, V. L. Zhdanov, Verification of chemical reaction rate models in turbulent reacting flows at Schmidt number considerably exceeding 1, J. Eng. Phys. Thermophys. 83 (3) (2010) 513–524.

[24] R. S. Barlow, C. D. Carter, Relationships among nitric oxide, temperature, and mixture fraction in hydrogen jet flames, Combust. Flame 104 (3) (1996) 288–299.

[25] R. S. Barlow, G. J. Fiechtner, C. D. Carter, J. Y. Chen, Experiments on the scalar structure of turbulent $CO/H_2/N_2$ jet flames, Combust. Flame 120 (4) (2000) 549–569.

[26] J. D. Li, R. W. Bilger, Measurement and prediction of the conditional variance in a turbulent reactive-scalar mixing layer, Phys. Fluids A 5 (1993) 3255.

[27] R. J. Brown, R. W. Bilger, Experiments on a reacting plume-2. Conditional concentration statistics, Atmos. Environ. 32 (4) (1998) 629–646.

[28] N. Swaminathan, R. W. Bilger, Study of the conditional covariance and variance equations for second order conditional moment closure, Phys. Fluids 11 (1999) 2679.

[29] G. Brethouwer, F. T. M. Nieuwstadt, DNS of mixing and reaction of two species in a turbulent channel flow: A validation of the conditional moment closure, Flow Turbul. and Combust. 66 (3) (2001) 209–239.

[30] G. K. Batchelor, Small-scale variation of convected quantities like temperature in turbulent fluid Part 1. General discussion and the case of small conductivity, J. Fluid Mech. 5 (1959) 113–133.

[31] R. W. Bilger, Some aspects of scalar dissipation, Flow, Turbul. Combust. 72 (2-4) (2004) 93–114.

[32] R. W. Bilger, Turbulent jet diffusion flames, Prog. Energy Combust. Sci. 1 (2) (1976) 87–109.

[33] R. O. Fox, The spectral relaxation model of the scalar dissipation rate in homogeneous turbulence, Phys. Fluids 7 (1995) 1082.

[34] C. D. Pierce, P. Moin, A dynamic model for subgrid-scale variance and dissipation rate of a conserved scalar, Phys. Fluids 10 (1998) 3041.

[35] A. W. Cook, W. K. Bushe, A subgrid-scale model for the scalar dissipation rate in nonpremixed combustion, Phys. Fluids 11 (1999) 746.

[36] J. Mi, G. J. Nathan, The influence of probe resolution on the measurement of a passive scalar and its derivatives, Exp. Fluids 34 (6) (2003) 687–696.

[37] L. K. Su, N. T. Clemens, Planar measurements of the full three-dimensional scalar dissipation rate in gas-phase turbulent flows, Exp. Fluids 27 (6) (1999) 507–521.

[38] A. N. Karpetis, R. S. Barlow, Measurements of scalar dissipation in a turbulent piloted methane/air jet flame, Proc. Combust. Inst. 29 (2) (2002) 1929–1936.

[39] L. K. Su, D. B. Helmer, C. J. Brownell, Quantitative planar imaging of turbulent buoyant jet mixing, J. Fluid Mech. 643 (2010) 59.

[40] P. Kailasnath, K. R. Sreenivasan, J. R. Saylor, Conditional scalar dissipation rates in turbulent wakes, jets, and boundary layers, Phys. Fluids A 5 (1993) 3207.

[41] J. R. Bourne, C. Hilber, G. Tovstiga, Kinetics of the azo coupling reactions between 1-naphthol and diazotised sulphanilic acid, Chem. Eng. Commun. 37 (1-6) (1985) 293–314.

[42] R. V. Mehta, J. M. Tarbell, An experimental study of the effect of turbulent mixing on the selectivity of competing reactions, AIChE J. 33 (7) (1987) 1089–1101.

[43] I. Nakamura, Y. Sakai, M. Miyata, Diffusion of matter by a non-buoyant plume in grid-generated turbulence, J. Fluid Mech. 178 (1987) 379–403.

[44] T. Watanabe, Y. Sakai, K. Nagata, O. Terashima, T. Kubo, Simultaneous measurements of reactive scalar and velocity in a planar liquid jet with a second-order chemical reaction, Exp. Fluids 53 (5) (2012) 1369–1383.

[45] T. Watanabe, Y. Sakai, K. Nagata, O. Terashima, Joint statistics between velocity and reactive scalar in a turbulent liquid jet with a chemical reaction, Phys. Scr. T155 (2013) 014039.

[46] Y. Sakai, I. Nakamura, T. Kubo, An experimental study on the consecutive and competing reaction in a turbulent liquid jet by the light absorption spectrometric method, in: Proc. Eleventh Symp. on Turbulent Shear Flows, Grenoble, France, 1997, pp. 18–19.

[47] V. Zhdanov, A. Chorny, Development of macro-and micromixing in confined flows of reactive fluids, Int. J. Heat Mass Transfer 54 (15) (2011) 3245–3255.

[48] T. Watanabe, Y. Sakai, K. Nagata, O. Terashima, Experimental study on the reaction rate of a second-order chemical reaction in a planar liquid jet, AIChE J. 60 (11) (2014) 3969–3988.

[49] T. Watanabe, Y. Sakai, K. Nagata, O. Terashima, H. Suzuki, T. Hayase, Y. Ito, Visualization of turbulent reactive jet by using direct numerical simulation, Int. J. Model. Simul. Sci. Comput. 4 (2013) 1341001.

[50] T. Watanabe, Y. Sakai, K. Nagata, Y. Ito, T. Hayase, Wavelet analysis of coherent vorticity near the turbulent/non-turbulent interface in a turbulent planar jet, Phys. Fluids 26 (9) (2014) 095105.

[51] T. Watanabe, Y. Sakai, K. Nagata, Y. Ito, T. Hayase, Vortex stretching and compression near the turbulent/nonturbulent interface in a planar jet, J. Fluid Mech. 758 (2014) 754–785.

[52] T. Watanabe, Y. Sakai, K. Nagata, Y. Ito, T. Hayase, Enstrophy and passive scalar transport near the turbulent/non-turbulent interface in a turbulent planar jet flow, Phys. Fluids 26 (10) (2014) 105103.

[53] M. R. Roomina, R. W. Bilger, Conditional moment closure (CMC) predictions of a turbulent methane-air jet flame, Combust. Flame 125 (3) (2001) 1176–1195.

[54] M. Fairweather, R. M. Woolley, First-order conditional moment closure modeling of turbulent, nonpremixed methane flames, Combust. Flame 138 (1) (2004) 3–19.

[55] S. B. Pope, PDF methods for turbulent reactive flows, Prog. Energy Combust. Sci. 11 (2) (1985) 119–192.

[56] J. D. Li, R. W. Bilger, A simple theory of conditional mean velocity in turbulent scalar-mixing layer, Phys. Fluids A 6 (1994) 605.

[57] H. Feng, M. G. Olsen, R. O. Fox, J. C. Hill, Conditional statistics for passive-scalar mixing in a confined rectangular turbulent jet, Phys. Fluids 19 (2007) 055104.

[58] S. H. Kim, H. Pitsch, Mixing characteristics and structure of a turbulent jet diffusion flame stabilized on a bluff-body, Phys. Fluids 18 (2006) 075103.

[59] N. Peters, F. A. Williams, Liftoff characteristics of turbulent jet diffusion flames, AIAA J. 21 (3) (1983) 423–429.